IMPACT OF MANGROVE ON TIDAL PROPAGATION IN A TROPICAL COASTAL LAGOON

Marcellin Samou Seujip, Xavier Bertin, Issa Sakho, Mouhamadoul Bachir Diouf

IMPACT OF MANGROVE ON TIDAL PROPAGATION IN A TROPICAL COASTAL LAGOON

Marcellin SAMOU SEUJIP[1,2], Xavier BERTIN[2], Issa SAKHO[3,4], Mouhamadou Bachir DIOUF[1]

[1] Laboratoire de Sédimentologie et de Biostratigraphie, Faculté des Sciences et Techniques, Université Cheikh Anta DIOP de Dakar, BP : 5005 Dakar-Fann, Sénégal
[2] UMR 7266 Littoral Environnement et Sociétés (LIENSs), CNRS - La Rochelle Université, 2 rue Olympe de Gouges France.
[3] Université Amadou Mahtar MBOW de Dakar à Diamnadio, UMR Sciences, Technologies Avancées et Développement Durable, BP 45927. Dakar – Sénégal
[4] NormandieUniv, UNIROUEN, UNICAEN, UMR CNRS 6143 M2C, 76000 Rouen, France

ABSTRACT :

Very complex aquatic ecosystem, the mangrove forest colonizes coastal lagoons, estuaries and deltas in tropical and subtropical zones. This study investigates the impact of mangrove vegetation on tidal propagation in the Somone Coastal Lagoon, located on the Senegalese small coast. The analysis of new field data is complemented with the application of a 3D circulation model accounting for vegetation. The analysis of well-reproduced water levels and currents over the whole lagoon make it possible to spatially study the amplitudes of the main tidal harmonics, semi-diurnal (M_2), diurnal (K_1) and the major overtide (M_4). The comparison between our baseline model accounting for vegetation and a configuration without vegetation reveals firstly that the mangrove strongly attenuates tidal propagation in the lagoon, whit a stronger impact on semi-diurnal waves than diurnal waves. Tidal currents are also strongly reduced when the mangrove is accounted for, even close to the inlet mouth, far away from vegetation areas. The mangrove also enhances tidal asymmetry and promotes ebb dominance, both in terms of duration (ebbs last from 0.5 up to 3 h more than floods) and current magnitude (ebb currents are about 50% stronger). Spring tides accentuate ebb-dominance compared to neap tides, where tidal asymmetry is weaker.

Keywords: Coastal lagoon, Tidal propagation, Mangrove forest, Tidal asymmetry, SCHISM, Somone River.

1. INTRODUCTION

Coastal ecosystems such as lagoons, estuaries and deltas, are among the most productive aquatic environments in the world (Day et al. 1987; Kjerfve 1994; Miththapala 2013; El Mahrad et al. 2022), while they host a specific variety of fauna and flora. Tidal inlet and barrier island systems represent about 10-17% of the world coastlines (e.g., Stutz and Pilkey 2001; Stutz and Pilkey 2011). Coastal lagoons are impacted by both natural and anthropogenic processes (Webster and Harris 2004; Sakho et al. 2011; Sousa et al. 2009; Sakho et al. 2022). They often exhibit very high primary and secondary production rates and are valuable for fisheries, aquaculture, and sometimes for salt extraction (Kjerfve 1994). Worldwide, barrier coasts

usually backed by lagoons are particularly common along the African Coasts (17.9 % of the worldwide coastline barrier, Cromwell 1971; Barnes 1980; Kennish and Paerl 2010), with for instance a continuous sequence along the Atlantic Coast of Western Africa (Albaret and Diouf 1994). The dynamics of coastal lagoons is complex due to the combination of tide, short waves, river input, wind, precipitation to evaporation balance and surface heat balance. It is important to understand the impacts of the ever-changing natural forcing on the hydro-sedimentary dynamics and morphological development of coastal lagoons so as to ensure a sustainable management of these systems (Wang et al. 1999). In the eastern tropical Atlantic, the tide is symmetrical off the West African coast (Song et al. 2011; Núñez et al. 2020) and the possible development of an asymmetrical tide on the coasts is linked to non-linear effects (Friedrichs and Aubrey, 1988; Song et al. 2011). In open coastal lagoons, tides can dominate hydrodynamics over river flows although the associated dynamics is very complex. Tidal wave propagates in a shallow medium and because of non-linear interactions, deforms and becomes asymmetrical, modifying the intervals between the flood and the ebb as well as tidal currents (Dias et al. 2013). The interaction of a tidal constituent with itself or with others fundamental constituents generates overtides (e.g., M_4) and fortnightly (e.g., MsF) constituents. In deep inlets and estuaries where the total water depth varies little between low tide and high tide, mass conservation implies that shorter floods (resp. ebbs) result in stronger currents compared to ebbs (resp. floods), so that the inlet is flood-dominated (resp. ebb-dominated) in terms of sediment transport (Aubrey 1986; Friedrichs and Aubrey 1988; Friedrichs et al. 1992). This situation strongly contrasts with shallow inlets (i.e., when the ratio between the mean water depth and the tidal range is below unity) where longer ebbs are usually characterized by stronger currents than during flood, so that these systems can be ebb-dominated (Bertin et al. 2009; Brown and Davies 2010; Dodet et al. 2013). This paradoxical behavior is explained by a strong tidal distortion, where ebbs take place in much shallower water depths than flood so that mass conservation is preserved. The tidal asymmetry can affect the transport of any substance in addition to sediments such as plastic debris (Ji et al. 2022; Núñez et al. 2021). Aquatic vegetation also plays a significant role in near-shore hydrodynamics in many coastal areas (Brookes and Shields 1996; Norris et al. 2017; Zhang et al. 2020). Tidal dissipation by friction in mangrove environments can also lead to tidal asymmetry (Mazda et al. 1995; Aucan and Ridd 2000; Horstman et al. 2021). In the tropical band, many coastal lagoons are characterized by the presence of aquatic vegetation like mangroves. Mangrove ecosystems are unique transitional coastal ecosystems generally confined to the tropical and subtropical world regions in between 30°N and 30°S latitude (Giri et al. 2011). It is also well known that mangrove

habitats are super productive natural ecosystems (Spalding et al. 1997; FAO 2007) while they develop along about 75 % of tropical and subtropical coasts (Day et al. 1987), covering about 137,760 km^2 worldwide in year 2000 (Giri et al. 2011). When mangroves are in direct contact with the marine environment, they constitute a physical barrier and promote coastal protection by attenuating tide, swells energy, storms surge and tsunamis (Mazda et al. 1997; Saad et al. 1999; Dahdouh-Guebas et al. 2005; Dahdouh-Guebas and Koedam 2008; Horstman et al. 2014; Montgomery et al. 2018; Montgomery et al. 2019). Understanding mangrove forest interactions with hydrodynamics is important for the sustainable management of water resources, ecological functioning and flooding hazards. Submerged and emergent vegetation in shallow water significantly affects the flow and turbulence structure (Zhang et al. 2020). A notable characteristic of hydrodynamics of mangrove creeks is the asymmetry between the flood and ebb water velocity, often characterized by an ebb-dominance (Wolanski et al. 1980). Flow through emergent vegetation is largely governed by a balance between pressure gradients and vegetation drag with small length-scale turbulence produced by vegetation wakes (Nepf 1999; Nepf and Vivoni 2000; Zhang et al. 2020). Previous modeling studies focused on mangrove swamp system interactions with tidal propagation and the consequent effect of this vegetation on hydrodynamics (Mazda et al. 1995; Wolanski et al. 1990; Furukawa et al. 1997). For this purpose, a common way of modeling the effects of vegetation drag on currents is simply by applying an increased uniform bed roughness or a Manning coefficient in 2DH models (Aucan and Ridd 2000; Mazda et al. 1995; Wolanski et al. 1980; Kurniawan et al. 2014). However, this approach neglects important 3D effects such as differences between submerged and emergent vegetation on momentum (Lapetina and Sheng 2014; Zhang et al. 2020). In other analytical approaches, the quantification of momentum losses, either computed directly from the vegetation drag or indirectly with a representative vegetation roughness, comes from a spatially-averaged vegetation density and often assumes an element drag coefficient (Cd) constant (Temmerman et al. 2005; Baptist et al. 2007; Horstman et al. 2013; Horstman et al. 2015; Horstman et al. 2021). Among the possible approaches to account for mangrove in hydrodynamic simulations, Mazda et al (2005) related vegetation-induced drag forces to a vegetation density parameter. Many authors have advocated that 3D hydrodynamic models should better represent the vertical distribution of vegetation effects according to its density distribution (Mazda et al. 2005; Temmerman et al. 2005; Horstman et al. 2015; Zhang et al. 2020), to properly simulate the drag force and blockage on the flow structure in the mangrove swamp system or others aquatic vegetation. A lot of studies on vegetation-hydrodynamic interactions have already been conducted (e.g., Biggs et al. 2016; Moki et al. 2020; Zhang et al.

2020) but very few on the mangrove and even less at the scale of a coastal lagoon with an advanced representation in a 3D model. Based on a 3D numerical model, this study investigates the impact of mangrove vegetation on tidal propagation in a tropical shallow coastal lagoon mostly forced by tides. Interest is placed here on evaluating the modifications of tidal propagation (water levels, harmonic structure and resulting currents) both in areas without vegetation and inside mangrove. In the next section (section 2), the study area is presented, followed by a description of the methodology used for this study in section 3. In section 4, the results are presented and the outcomes of this study are finally discussed before some conclusions are drawn.

2. STUDY AREA

2.1 General Description

Located on the Senegalese *"Petite Côte"* (figure 1a, 1b) and bordered to the west by the Atlantic Ocean, the Somone Lagoon is a West African coastal lagoon (figure 1c) erected in Protected Marine Area since 2020. Sheltering an immensely rich biodiversity, it is a microtidal shallow (0-4 m) system set up during the Holocene period (Sakho 2011). The Somone River watershed extends over a surface area of 485 km². Belonging to the Sahelo-Soudanian tropical domain, the site is characterized by the alternation of two contrasting seasons: the dry season (November to May) and a shorter wet season (from June to October), where the mean rainfall is less than < 500 mm/yr since the 1960s). The dry seasonal regime is characterized by the predominance of the north, northeast and east winds and a humid seasonal regime dominated by western, southern and southwestern winds. The wet season is generally characterized by wind speeds below 4 m/s and in the dry season, wind speeds are sometimes twice as strong, 4 to 6 m/s (Sakho 2011). The lagoon system has four main morphological units: the mangrove forest, the inlet area, the mudflats and barren areas (sterile soils). One of the key features of this coastal lagoon is the development of the mangrove forest, which covers ~16% of its surface area (Sakho et al. 2011) with a dominance of Rhizophora. Close to the inlet, the mangrove disappears and morphological units typical of tidal inlets develop: a flood delta, a shallow channel controlled by bedrock outcrops to the north and a small and mostly subtidal ebb-delta. Unlike other sandspits in Senegal which are oriented southward following the dominant longshore transport, the sandy spit developing at the southern margin of the inlet is oriented northward, opposite to the south-eastward regional longshore transport but this dynamic is poorly known. For sediments grain size in Somone River, the sand fraction is dominant and

ranges from medium to fine sands near the inlet while mangrove areas are characterized by an accumulation of silts and clays (Sakho 2011).

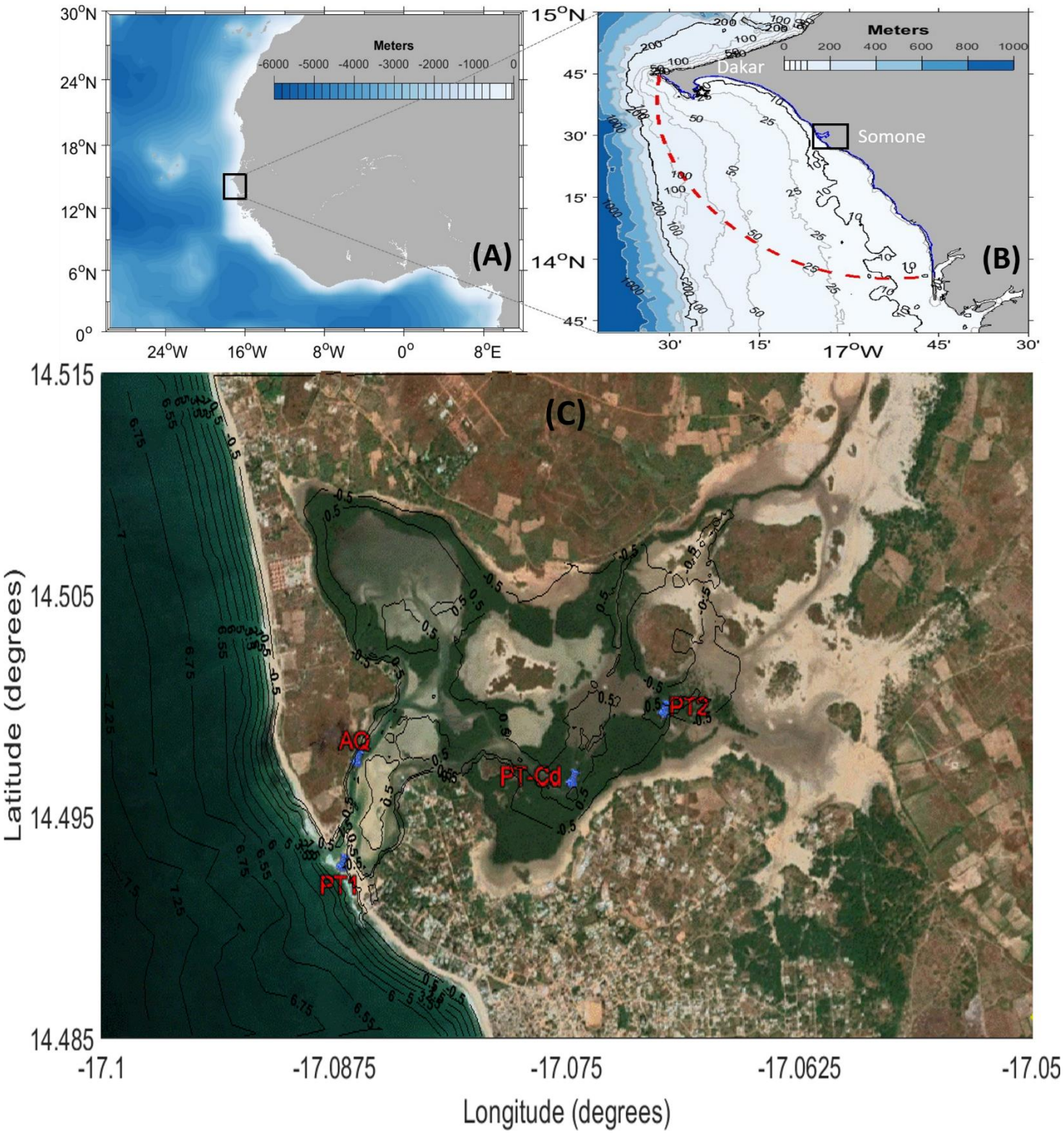

Figure 1: (A) Location of the study site on the small Senegal coast in West Africa, (B) Extension of the computational domain (sea boundaries in red dash-dotted line and land boundaries in blue) with the position of the Dakar tide gauge (black star) and (C) the Somone coastal lagoon with the position of measurement stations

and its local bathymetry. (The offshore bathymetry comes from Gebco (2019) and Geographical Datum WGS 84 is used for the georeferencing).

2.2 Hydrodynamic

The Somone lagoon is fed intermittently by a small river upstream, with a discharge ranging from 0 to 9.4 m^3/s (Sakho 2011). Due to the construction of several dams upstream, freshwater discharges in the lagoon are almost non-existent and negligible, partly linked to high water stress due to climate change (Sakho 2011). Therefore, hydrodynamic circulation is mostly driven by tides. The external tide off the Somone lagoon is symmetrical (Núñez et al. 2020). Tides are semidiurnal and range from 0.5 m to 2 m seaward but they suffer a strong dissipation inside the lagoon, although it has never been quantified. The water circulation in the lagoon flows through a little hierarchical channels and large tidal flats. Following the characteristic of Le Floch (1961), Somone lagoon is a hyposynchronous estuary.

3. METHODS AND DATA

3.1 Topographic and Bathymetric surveys

To characterize the morphology of the area of interest, several topographic campaigns were performed with DGPS (RTK GNSS). For the bathymetry, we used a single beam echosounder and carried out a bathymetric campaign in 2020 from October 20th to 26th, inside the lagoon and up 500 m offshore of the inlet. Beyond this marine limit, the General Bathymetric Chart of the Oceans (GEBCO 2019, https://download.gebco.net/) data were used. In this study, the vertical reference for the measurements taken is the Mean Sea Level (MSL) for both morphological and hydrodynamics data.

3.2 Hydrodynamic parameters: water level and current measurements

Hydrodynamic measurements were carried out in the lagoon at 2 different periods, first from the 21/10/2020 to the 04/11/2020 (14 days of continuous measurement at 2 Hz for water level and 2 min for currents), then from the 01/12/2020 to the 01/08/2021 (07 months) recording water level at a low frequency (10 min). To gradually follow the tidal wave from downstream to upstream of the lagoon system, the stations (figure 1c) chosen are: a sea station ‘PT1’ located approximately 100 m from the mouth (hereafter, SEA-PT1); a station ‘AQ’ at 500 m from the lagoon entrance (hereafter, Aquadopp); an upstream station ‘PT2’ (approximately 2.5 km from mouth) inside the mangrove (hereafter, Mangrove-PT2) and a last station ‘PT-Cd’ only used during low frequency observation at the intermediate downstream-upstream, in the deepest zone

of the system (hereafter, PT-Coude). The pressure sensors SEA-PT1 and Mangrove-PT2 were placed at the bottom and recorded at 2 Hz, while the Aquadopp (300 m depth rating, version 1.40.16) was located 0.6 m from the bottom and measured water pressure and currents averaged over 02 min. While deployed 0.6 m from the bottom, this Aquadopp integrated current velocities between 0.97 and 1.72 m from the bottom. Our study area benefits from the hourly tidal observations made at Dakar harbor (here after, Dakar Port) since 1960 (around 60 years, *https://uhslc.soest.hawaii.edu/stations/?stn=223#levels*). Regarding the Somone River upstream, although fresh water discharges were not measured during our field observations (from October to December 2020), they are considered negligible because the observation period correspond to the dry season, in addition to the presence of several dams as explained in section 2.2.

3.3 Numerical Modelling

3.3.1 SCHISM Model Presentation

For this study, we used the 3D Semi-implicit Cross-scale Hydroscience Integrated System Model (SCHISM, www.schism.wiki) to explore tide dynamics in the Somone coastal lagoon. It is an open-source community-supported modeling system based on unstructured grids, designed for seamless simulation of 3D baroclinic circulation across creek-lake-river-estuary-shelf-ocean scales (Zhang et al. 2016). This model is very efficient in terms of computational time and is widely used for similar coastal research studies (Picado et al. 2010; Dodet et al. 2013; Pein et al. 2014; Guerreiro et al. 2015; Zhang et al. 2016; Zhang et al. 2020; Oliveira et al. 2021). By solving the standard Navier-Stokes equations with hydrostatic and Boussinesq approximations, SCHISM uses a combination of a semi-implicit finite-element/finite-volume scheme and an Eulerian Lagrangian Method to treat the momentum advection, which guaranties a good balance between efficiently and numerical stability. Numerical computations are based on a flexible unstructured grid in the horizontal and both hybrid S-Z or LSC² grids in the vertical when used in 3D. The hydrostatic solver of SCHISM can be coupled with other modules incorporated in the modelling system such as sediment transport, short waves, water quality, oil spills and biology, etc. A detailed description of SCHISM, the governing equations and its numerical implementation can be found in Zhang et al (2016).

3.3.2 The Vegetation Module

SCHISM numerical model is capable of reproducing the complex 3D flow structure found near vegetated areas (Zhang et al. 2020). In submerged aquatic vegetation, the upper canopy produces vertical turbulent exchange with the overlying water and plays a significant role in the momentum balance and the lower canopy communicates with surrounding water predominantly through longitudinal advection (Nepf and Vivoni 2000). To add the vegetation friction parameter to the model numerical formulation, the Reynold's Averaged Navier-Stokes (RANS) equations are solved with an additional form drag term in the mean flow momentum equations and drag-induced turbulence production terms in the turbulence closure equations, in order to account for turbulence generated by either emergent or submerged vegetation (cf. Eqs. (7) and (8) in Zhang et al. 2020). The model uses a semi-implicit time stepping method and treats the vegetation-related terms implicitly to enhance numerical stability (Zhang et al. 2020). The stability is independent of the vegetation parameters, and the strong shear around the vegetation is efficiently simulated. The time step does not need to be reduced as compared with simulations without vegetation (Zhang et al. 2020). Until now, the explicit treatment of the very strong vegetation-induced friction terms involved reducing the time steps considerably and the computation time was increased by one order of magnitude (Temmerman et al. 2005; Horstman et al. 2014; Beudin et al. 2017a; Beudin et al. 2017b). The practical requirements for the SCHISM vegetation module include a drag coefficient, the canopy height, the stem density, and diameter (Zhang et al. 2020), both stem density and diameter being multiplied to give effective drag area per unit volume. The parametrization of vegetation proposed by Zhang et al (2020) relies on stems parameters, which are easier to parameterize compared to leaves or roots. In treating the vegetation as arrays of solid cylinders, they authors consider that it is only a first-order approximation of the problem. Other behaviors of vegetation, such as flexibility, sheltering effects are not yet incorporated to this module.

3.4 Model Implementation

The model domain extends about 200 km along the coast (from the Dakar peninsula in the North to Palmarin to the South (figure 1a)), encompassing a large part of the small Senegalese coast, and between 10-60 km in the cross-shore direction. The computational horizontal unstructured grid used consists of 25247 nodes for 48824 elements with triangular meshes ranging from 2 to 3 km offshore, between 200 m to 50 m when approaching the coastline (figure 1b) and a finer resolution on the Somone lagoon (8 m for the tidal channels; 10-20 m for the sandbank and between 20-30 m in the mangrove and intertidal flat areas). This grid takes into account areas that may be flooded beyond the maximum tide, as land elevations

of up to 2m above mean sea level have been covered. The vertical grid used here is Sigma-generalized (SZ) coordinates and has 10 levels. Additionally, the bathymetry at inaccessible places (too muddy, loss of signal of the RTK GNSS during recording due to the proximity of the mangrove) in the lagoon, was estimated by the water line method of Khan et al (2019) applied to Sentinels 2 images and water levels measured inside the lagoon at PT-Coude. For the duration of the water level observations at PT-Cd, all available Sentinel 2 images of the lagoon with low nebulosity were first collected, such as to digitalize the waterline limit outside mangrove swamps. For each digitized limit, a bathymetry corresponding to the equivalent water level observed at the PT-Cd was assigned. A total of 14 different lines were thus obtained for distinct tide periods, covering vast intertidal spaces. The model is run in 3D barotropic mode, and forced along its open boundary by the 13 main astronomical constituents linearly interpolated from the regional model FES2012 *(*Carrère et al. 2012*)*. Based on water level recordings from the Dakar tide gauge, a study of mean sea level variation showed a substantial variability of mean sea-level, characterized by a seasonal cycle over which an upward trend of 2.71 mm/yr (~3 mm/yr) is superimposed. Given that the model was validated over a relatively short period (2 weeks), mean sea level at the open boundary was considered constant in this study. The model does not take into account any freshwater supply from the Somone upstream River in this configuration. Over the whole domain, the circulation model is forced by tri-hourly 10 m wind speed and sea-level pressure fields from the Climate Forecast System Reanalysis CFSR (Saha et al. 2010). The datasets are provided on a regular grid with a similar spatial resolution of 0.5° x 0.5° for the wind and the atmospheric pressure. After calibration of the circulation model, the bed roughness in this 3D configuration is set to 0.0001 m in the open ocean and ranges from 0.0001 m to 0.002 m in the lagoon (depending on the bottom nature and the expected presence of bedforms in the channels). As the tide gauge of Dakar is directly connected to the open ocean, this station was used first to evaluate offshore tides in the model. The spatial repartition of roughness length Z0 was then adjusted through model/data comparison for water levels around the inlet mouth (station PT1 and AQ), applying values commonly found in the literature for tidal flats (0.0001 m) and tidal channels (0.002 m) where bedforms are expected to develop. Next, the measured properties of the vegetation (stem density and diameters) were applied to the vegetation module and the drag coefficient in these areas was adjusted through model-data comparison at the PTs located inside mangrove areas (PT-Cd and PT2). Considering the mangrove friction parametrization, density estimation of vegetation area was done first from in situ measurement of diameter and height based on trees roots and stems. This parametrization was extended spatially based on Sentinel 2 imagery mentioned

above, which were used to map the mangrove extention over the whole Lagoon. Mangrove stem densities used here correspond to 127 ± 16 stems/m^2 (where ± corresponds to one standard deviation). The propagules, the roots and the trunks are all averaged according to a parameterization of mass in cylindrical stem (with diameter of 5 ± 0.59 cm). In this parameterization, the leaves are not taken into account considering that the mangrove canopy is about 3 m above MSL and only the roots and stems are in contact with water during a tidal cycle. To adequately represent the friction related to mangrove vegetation, a sensitivity analysis was performed, where Cd was varied from 0.1 and 1 with a 0.025 interval and a uniform value was applied for the entire mangrove. This calibration process resulted in an optimal drag coefficient (Cd) of 0.25. Ultimately, the model was validated through current velocities at station AQ, as they both depend on the parameterization of roughness length around the inlet and the parameterization of vegetation in mangrove areas. The time step was set to 10 s and the simulations start from 20/10/2020 to the 20/12/2020. This simulation duration equivalent to 2 times the lunar month is long-enough to separate the main tidal constituents by means of harmonic analysis (U-Tide, Codiga 2011). Simulating this two-month period takes 12 hours on 80 cores.

3.5 Assessing the impact of mangrove

In order to assess the impact of the mangrove on tidal dynamics inside the lagoon, a second model configuration was implemented, where no mangrove is represented in the lagoon while all other parameters are kept constant. The computational time without accounting for vegetation was only reduced by about 10%, in agreement with Zhang et al (2020). The differences in terms of water levels and current velocities observed between these two simulations were used to evaluate the impact of mangrove on tidal propagation inside the lagoon. To spatially quantify the mangrove effects on tidal dissipation and distortion, the main semi-diurnal (M_2), quarter diurnal (M_4) and diurnal (K_1) tidal constituents were computed from U-Tide (Codiga 2011), for both model configurations. Thereafter, we focused analysis to harmonics M_2, M_4 as they are sufficient to characterize tidal asymmetry in estuaries and lagoons. The amplitudes ratio (AM_4/AM_2) of M_4 and M_2 constituents can be used as a quantification of tidal distortion, while their compound phase ($2\varphi_{M2} - \varphi_{M4}$) detects the nature of the asymmetry as established by previous studies (Friedrichs and Aubrey 1988; Zapata et al. 2019). According to these authors, a ratio $AM_4/AM_2 > 0.01$ indicates an important distortion in the tidal wave. Regarding the value of the compound phase, if $0° < 2\varphi_{M2} - \varphi_{M4} < 180°$, the flow is flood-dominant, otherwise if $180° < 2\varphi_{M2} - \varphi_{M4} < 360°$, the flow is ebb-dominant.

4. RESULTS AND DISCUSSION

4.1 Model predictive skills and limitations

4.1.1 Water levels

The tidal model implemented in the Somone lagoon fairly reproduces water levels both in the open sea and inside the lagoon system when vegetation is accounted for. Model data comparison shows a good match between observed and modelled water levels (figure 2), with root mean square discrepancies (RMSD) of approximately 0.05 m for the sea stations (Dakar Port (0.048 m) and off the Somone River, SEA-PT1 (0.056 m)); 0.046 m at the entrance to the Lagoon (at Aquadopp), and about 0.098 m in the mangrove areas (at Mangrove-PT2). The normalized root mean square discrepancies (hereafter NRMSD) shows that the error grows from about 5 % seaward and up to Aquadopp and grows to 9.6 % in the mangrove part upstream (at Mangrove-PT2).

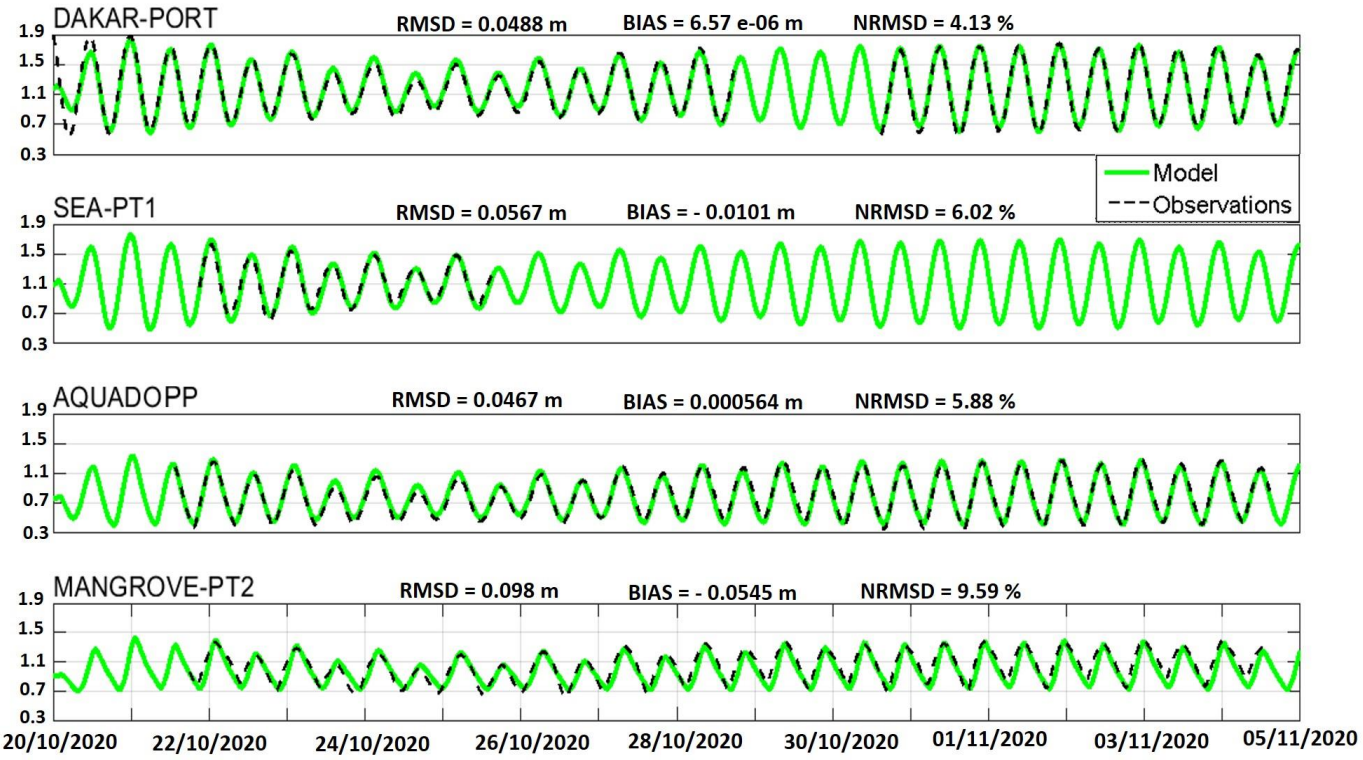

Figure 2: Comparison between observed (black dotted line) and modelled water levels in Dakar reference tide gauge station (Dakar-Port), and Somone measurement stations at Sea (Sea-PT1), at the lagoon entrance (Aquadopp) and upstream inside mangrove (Mangrove-PT2).

4.1.2 Currents

In order to perform a consistent comparison, modeled currents were integrated over the same depth as the Aquadopp (see section 3.2). Similarly to water levels, currents obtained from the model are in good agreement with the field observations. As shown in the figure 3, eastward U (m/s) and northward V (m/s) current components are better reproduced at the end of the ebb (and flood beginning) than at the end of the flood (and ebb beginning). The resulting RMSD is 0.0468 m/s for the eastward and 0.0127 m/s for the northward components and their corresponding NRMSD are 7.8 % and 10.6 % respectively. The model presents a bias on ebb peaks which are over-estimated by 0.1-0.15 m/s.

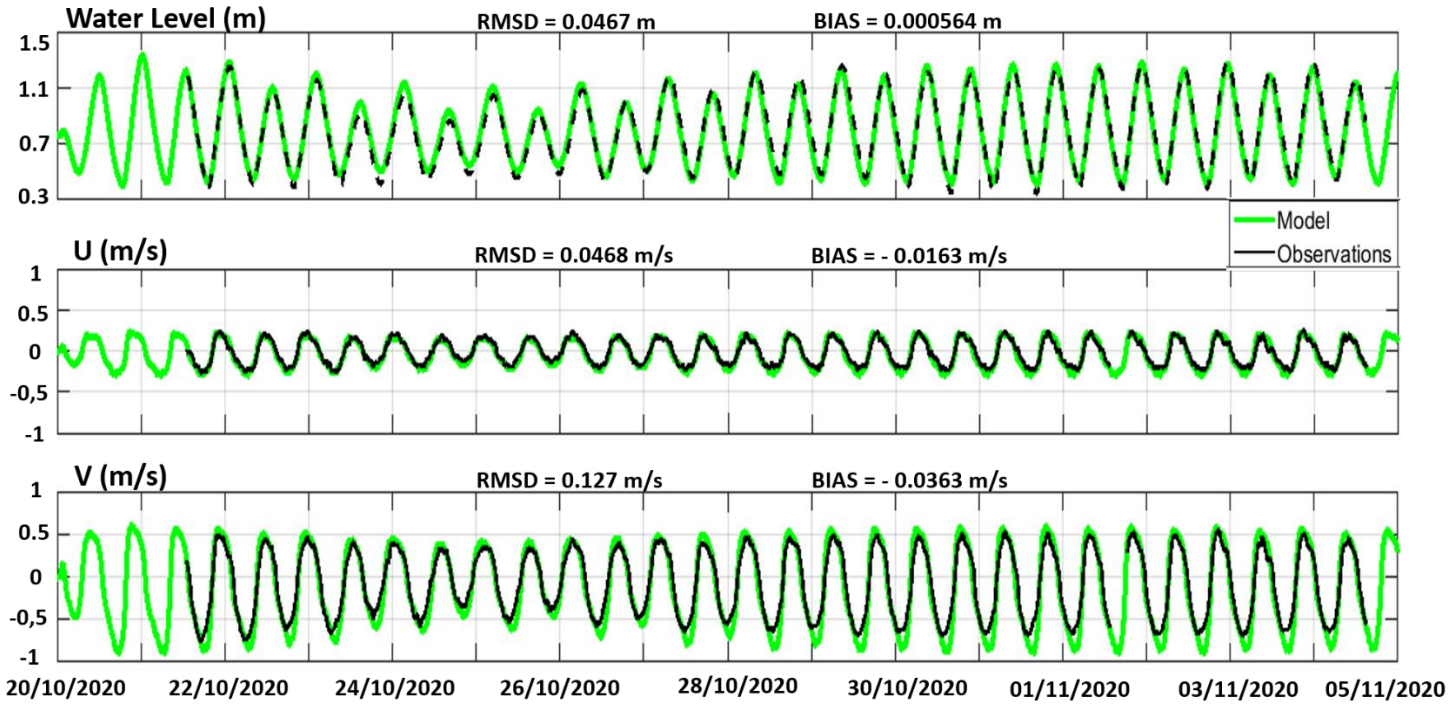

Figure 3: Comparison between observed (black) and modelled (green) water levels (up), Eastward (middle) and Northward (down) currents at the Aquadopp station, located vertically at 0.6 m from the bottom.

4.1.3 Limitations of the present model

Model/data comparison showed that the model was able to reproduce tidal propagation in this complex coastal system with an accuracy comparable with previously published studies in estuaries and coastal lagoons with (e.g., Sathyanathan and Deeptha 2013, Zapata et al. 2019) or without mangrove (Dodet et al. 2013). Nevertheless, water levels are less accurately reproduced in the mangrove upstream of the system, with a NRMSD at PT2 twice as large as at the entrance of the lagoon. These larger errors can originate from several sources, including the bathymetry or, the choice of parameters used to represent the mangrove (Cd and stem properties). Indeed, in the channels bordering areas of mangroves, the surveyed bathymetric

profiles are locally too distant while no data at all were collected inside the mangrove. To better quantify the impact of these limitations, sensitivity analyses were done raising or deepening the bathymetry by 1 m in these areas but the results were little conclusive. Regarding vegetation, one can expect that spatially-uniform values for Cd and stem dimensions and densities are locally not adequate, namely because two different species develop inside the lagoon (avicennia and rhizophora). Furthermore, Mazda et al (2005) and Horstman et al (2021) showed that using a variable spatial drag coefficient, both vertically and horizontally, can improve the modelling of the hydrodynamics in such environments. Also, the present parametrization proposed in the vegetation module used in this study remains too simplistic to represent the hypercomplex structure of the mangrove and consequently remains only a first-order approximation of the problem. In future studies, the impact of a spatially-varying representation of the mangrove (both horizontally and vertically) will have to be investigated (e.g., Mazda et al. 2005; Shan et al. 2019; Horstman et al. 2021; Yoshikai et al. 2022), although requiring very detailed hydrodynamic measurements, challenging to perform in such environments. Finally, the effects of short waves are not considered in the present modelling approach while several studies already showed that the dissipation of short waves at the entrance of coastal lagoons can drive a setup reaching about 5 to 10% of the wave height at breaking (Oliveira et al. 2006; Nguyen et al. 2007; Bertin et al. 2009; Olabarrieta et al. 2011; Dodet et al. 2013; Bertin et al. 2015; Lavaud et al. 2020). In the present study, a detailed model/data comparison at the Aquadopp and PT2 stations reveals that the model underestimates water levels by 0.05 to 0.10 m between October 28th and 30rd (figure 3, panels c and d) while the ERA5 reanalysis suggests that the offshore significant wave height increased from 0.5 to 1.2 m during this period. This comparison suggests that short waves can have a relevant contribution to the hydrodynamics of the lagoon and will have to be accounted for in future hydrodynamic studies. However, the study area is exposed to swells originating from both the North and the South Atlantic Ocean, often resulting in multimodal sea states. Therefore, including short waves in the model would require computing time series of 2D spectra along the open boundary of the model, which is under progress. Finally, Sakho (2011) showed that the lagoon is an inverse estuary with an increase in salinity due to evaporation from downstream to upstream of the system while water temperature is also increasing upstream. This singular behavior could drive baroclinic effects, which are not considered in the present study.

4.2 Tide-induced hydrodynamics of the lagoon (tidal range, tidal distortion)

The stations at sea, the Dakar Port and Sea-PT1 show very similar tidal ranges (from 0.5 m to 1.3 m), but it decreases to 0.4-1 m inside the lagoon at Aquadopp and further to 0.3-0.7 m inside mangrove areas (figure 2). The hyposynchronous nature of the Somone lagoon is well shown by this decreasing tidal range from downstream to upstream. The tide observed in Dakar (Dakar-Port) and off Somone (PT1) is symmetrical, while inside the lagoon it suffers a significant distortion which intensifies from downstream to upstream in the mangrove. Ebbs durations are always longer than floods ranging from 0.5 h up to about 2 h at Aquadopp and from 0.5 h up to 3 h in PT2-mangrove. The observed distortion is more pronounced during spring tides. Regarding tidal propagation at the mouth, the duration where flood currents are established ranged from 5.5 and 6 hours while ebb currents were established between 6.5 and 7.5 hours at the location of the Aquadopp (figure 3). From the observations, the northward current component (main flow direction) ebb currents are about 50% stronger than flood currents, while for the eastward component, flood and ebb currents are of similar amplitude (figure 3).

4.3 Mangrove impacts on tidal propagation

In this section, we compared our baseline simulation with the simulation without mangrove in order to assess the effect of vegetation on tidal propagation.

4.3.1 Mangrove effect on the water level asymmetry

The water level comparisons from these 2 configurations (with and without mangrove) at the lagoon mouth (Aquadopp) and upstream inside the mangrove (Mangrove-PT2) is shown in Figure 4. Without vegetation, the tidal amplitude is excessive in the model and results in a 20-30% stronger RMSD. Due to the absence of attenuation by vegetation, larger errors are found in lagoon areas close to mangroves. Previous studies also reported the dissipation of tides as it propagates through vegetation (McIvor et al. 2012, Montgomery et al. 2018, Moki et al. 2020; Zhang et al. 2020).

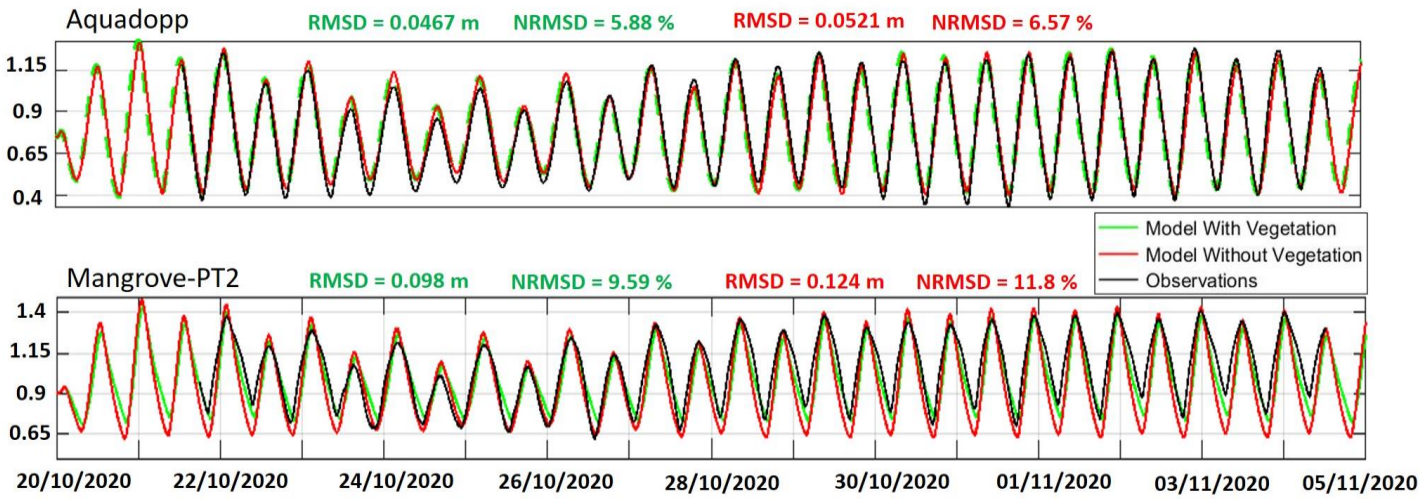

Figure 4: Comparison of water levels in the lagoon, mouth entrance (Aquadopp) and upstream inside mangrove (Mangrove-PT2) based on 02 model configurations, with vegetation (green) and without vegetation (red) and observations (black).

4.3.2 Mangrove effect on tidal currents

Tidal dissipation by mangrove forest in the lagoon is also well highlighted by the magnitude of the currents, which are substantially overestimated without vegetation (figure 5), with a RMSD increased by 60 %. In more details, accounting for vegetation has a much larger impact on flood currents than ebb currents, so that the asymmetry in current velocity is much reduced when neglecting vegetation. The spatial extension of this behavior will have to be investigated in future studies, as well as its impact on sediment transport.

Montgomery et al (2018) and Horstman et al (2015) both relayed that the mangrove drag effect is linked to the flow nature (creek and sheet flow). Sheet flow corresponds to the transportation over the vegetated platform through the mangroves, which becomes increasingly important with reduced channelization and at increasing water levels while creek flow dominates in channelized mangroves at low water levels (Montgomery et al. 2018). For sheet flow, Montgomery et al (2018) showed that vegetation properties were important by impeding water exchange across the forest, reducing water levels and slowing down the flood wave propagation in agreement with our results, while for creek flow, the authors highlighted a minimal mangrove contribution to the flow restriction. In the Somone Lagoon, because of the spatial mangrove distribution, tidal circulation allows both sheet and creek flow. Tidal dissipation by the mangrove appears to be related to the water level inside the mangrove, with a stronger dissipation by the mangrove during spring tides (e.g., from 28/10 to 05/11 cf. figure 4, Mangrove-PT2) and a lower tidal dissipation by mangrove during neap tides (e.g., from 24/10

to 27/10 cf. figure 4, Mangrove-PT2) when the tide penetrates very little into the mangrove. A similar behavior was previously obtained by Kitheka (1997) inside mangrove area in Gazy Bay (Kenya).

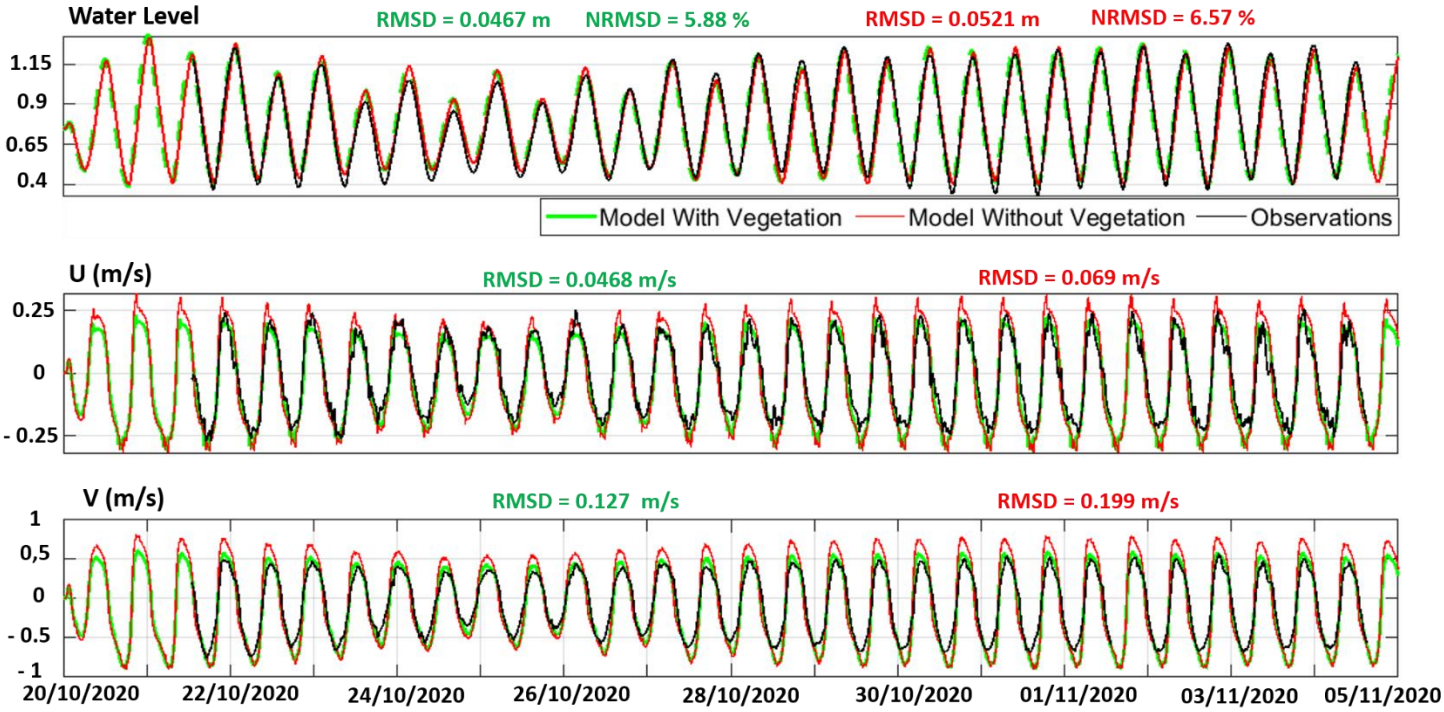

Figure 5: Comparison of current components in the lagoons, at the mouth entrance (Aquadopp station) based on 02 model configurations, with vegetation (green) and without vegetation (red) and observation (black). Top panel (water level), middle (U (m/s)) and bottom (V (m/s)).

Contrary to the result obtained by Wu et al (2001) in the Merbok Estuary (Malaysia), showing rather a decrease in both flood and ebb currents in a configuration without mangroves compared to the case of taking into account the mangrove where they observed an acceleration of the floods and ebbs currents in channels, our study shows weaker currents when the mangrove is represented (figure 5). However, both studies are supported by local measurements, which makes difficult any generalization.

4.4 Effects of the mangrove on tidal dissipation

To spatially assess the mangrove effects on tidal dissipation at the lagoon scale, the main tidal harmonic constituents are compared in the presence and absence of vegetation (Figure 6). The amplitude differences between the two simulations were normalized in order to spatially quantify the dissipation inside the lagoon for each constituent (Figure 6, right panels). Both with and without vegetation, the semi-diurnal tidal wave M_2 first decreases from 0.45 m to

about 0.35 m (~30 %) when propagating through the inlet, a process well documented in other similar shallow inlets (e.g., Bertin et al. 2009; Dodet et al. 2013). When entering the mangrove, M_2 further decreases down to 0.3 m or less when the vegetation is accounted for, while it remains constant when vegetation is not represented. The mangrove vegetation is responsible for an important dissipation of M_2, which ranges from 25% and more than 40% (~45% maximum) upstream and from 20% to 10% in the central part of the lagoon. The slight increase of the amplitude of M_2 and K_1 near the inlet mouth is explained by a higher MSL inside the lagoon when the mangrove is accounted for in the model. This increase in MSL reaches 0.05 m under spring tides, which could appear small but locally represents a 10% increase in water depth close to the inlet mouth near low tide. Diurnal tidal waves suffer much less dissipation when propagating through the inlet and decrease only by a few percent. When reaching mangrove areas, diurnal waves also suffer less dissipation than semi-diurnal waves and their amplitude only decreases by 5 to 15% with the maximum dissipation upstream. On the opposite, the M_4 overtide mostly develops inside the lagoon and continuously increases from the inlet region to the upstream part of the lagoon, except at the most distant channel to the NE of the lagoon. Unlike diurnal and semi-diurnal waves, the amplitude of M_4 increases by 25 to 50 % when the vegetation is accounted for.

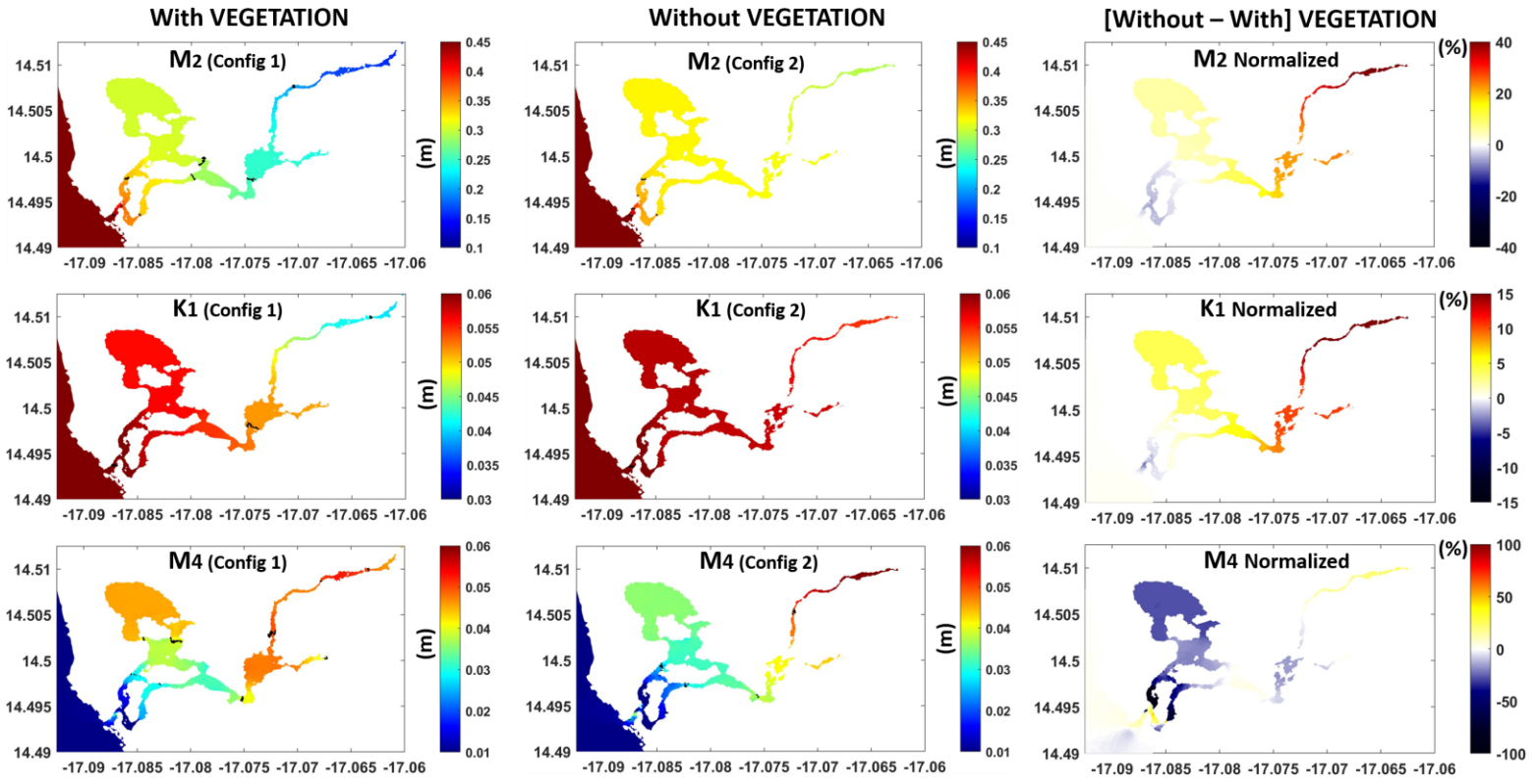

Figure 6: Spatial amplitudes of tidal harmonics M_2, M_4 and K_1 in Somone lagoon in 02 different model configurations, (left panels) configuration with mangrove (vegetation) and (middle panels) configuration without mangrove, and their respective amplitude differences normalized (right panels) between the configurations with and without vegetation. (Black isolines are spatially presented every 0.05 m for M_2 and 0.01 m for both K_1 and M_4).

4.5 Effects of the mangrove on tidal distortion

In both simulations, the ratio AM_4/AM_2 is of the order of 10%, which indicates a substantial distortion of the tidal wave inside the lagoon (figure 7, top panel). In more details, the comparison between the simulation with and the simulation without vegetation clearly shows that the mangrove enhances tidal distortion, with a ratio AM_4/AM_2 increased by 30 to 50%. This reduction in tidal asymmetry for water levels without mangrove corroborates well the asymmetry on tidal currents, with maximum flood currents almost as strong as maximum ebb currents without mangrove presented in figure 5. The analysis of the compound phase $(2\varphi_{M2} - \varphi_{M4})$ shows values of the order of 355° inside a large part of the lagoon (figure 7, bottom panel), which is well above 180° and implies ebb-dominance for both configurations with and without vegetation. In more details, both configurations also show similar characteristics at the inlet mouth ($(2\varphi_{M2} - \varphi_{M4})$ is of the order of 320°), but without mangrove, at lagoon downstream, the ebb dominance seems to be weaker ($(2\varphi_{M2} - \varphi_{M4})$ shows values of the order of 300°). Overall, the compound phase $(2\varphi_{M2} - \varphi_{M4})$ is higher over the main part of the lagoon when vegetation is accounted for, which leads to a greater distortion of the tidal wave by the mangrove.

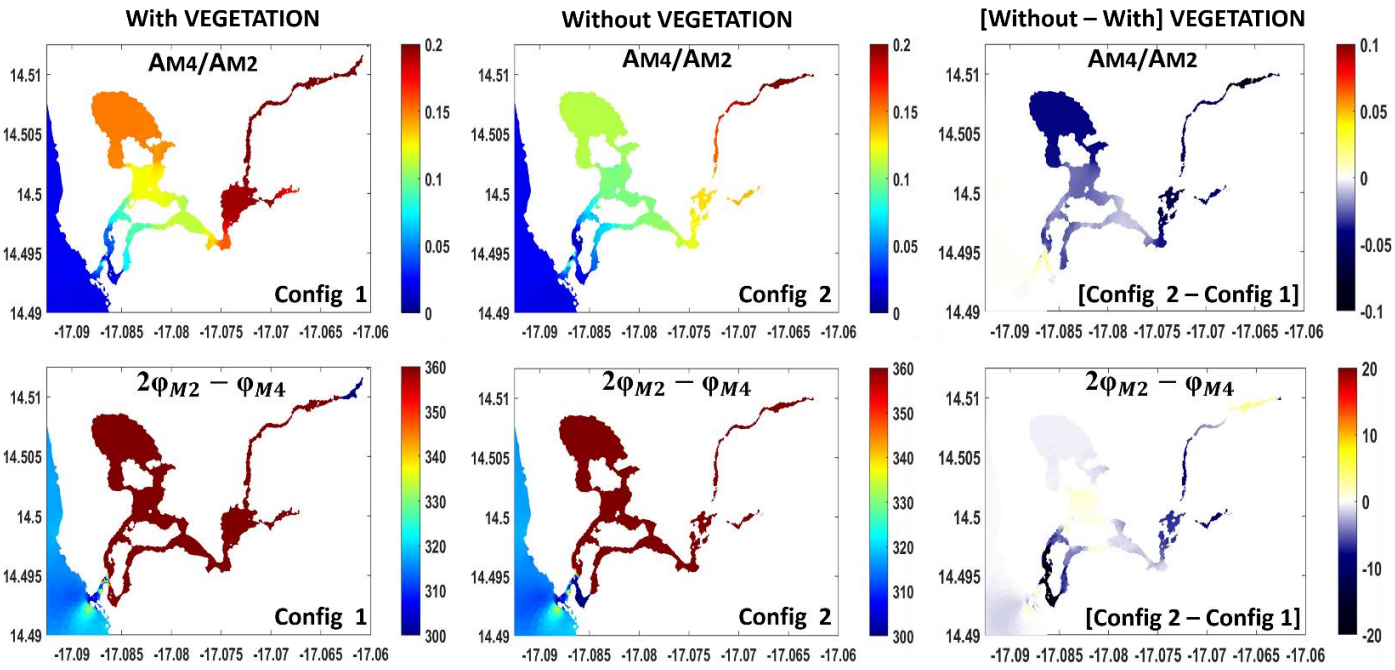

Figure 7: Spatial amplitudes ratio of harmonics AM_4/AM_2 constituent and their compound phases $2\varphi_{M2} - \varphi_{M4}$ in Somone lagoon in 02 different model configurations, (left) configuration with mangrove (vegetation) and (middle) configuration without mangrove, and their respective differences obtained between the configuration without and with vegetation (right panels).

Somone Lagoon presents a contrasting behavior according to the classical theories of Friedrichs and Aubrey (1988) on tidal asymmetry. Thus, in the lagoon, larger velocities occur during the ebb, while ebb lasts more than flood. As seen in the introduction, this paradoxical behavior is explained by the strong tidal distortion, where ebbs take place in much shallower water depths than flood, so that mass conservation is preserved (e.g., Bertin et al. 2009). While this strong ebb-dominance is well explained by the propagation of the tidal wave in a channelized shallow environment with intertidal flats slightly above mean sea level (e.g., Fortunato and Oliveira 2005), this study also showed that ebb-dominance was further enhanced by the presence of vegetation. Others relevant studies already reported a similar enhancement of ebb-dominance due to the mangrove (Wolanski et al. 1980; Lessa and Masselink 1995; Mazda et al. 1995). In these studies, the authors proposed that the large volume of water that inundates the mangrove area at high tide is progressively released during the ebb, which enhances ebb-dominance. As more, water is trapped by the mangrove during high tides, this process is exacerbated during spring tide. Others relevant studies also reported the fact that tidal waters remained perched for long inside the mangrove swamp during ebbs (e.g., Wolanski et al. 1980; Wolanski 1992; Aucan and Ridd 2000). Much stronger ebb-currents certainly promote ebb-dominance in terms of sediment transport, which could explain that the Somone Lagoon remained open most of the time over the last decades (Sakho 2011). This hypothesis will have to be verified in the future, for instance through the morphodynamic modelling of the lagoon, accounting for short waves which can promote inlet closure during storms (e.g., Bertin et al. 2009; Dodet et al. 2013).

5. CONCLUSION

The impact of mangrove on tidal propagation in a tropical coastal lagoon was assessed in this study based on new field observations complemented with a 3D numerical model, where the vegetation is parameterized by means of a drag coefficient and stem properties. Once the vegetation is correctly represented, the model showed good predictive skills to reproduce tidal propagation, dissipation and distortion in the lagoon, which further allowed to quantify the impact of mangrove. The harmonic analysis of modelling results revealed a strong dissipation

of semi-diurnal waves, first at the passage of the inlet and next in vegetated areas. Comparatively, diurnal tidal waves suffer much less dissipation, both at the inlet and inside the mangrove. On the opposite, the quarter-diurnal wave M_4 mostly develops inside the lagoon and is strongly enhanced when the mangrove is represented. Thus, the amplitude ratio AM_4/AM_2 is up to two times larger in the presence of vegetation. In terms of tidal currents, strongly distorted water levels result in a strong ebb-dominance, with ebb currents 50% larger than flood currents at the location of our measurements when vegetation is accounted for. The detailed analysis of both modelling results and field data also revealed that tidal asymmetry if much stronger during spring tides, probably because tides little penetrate the mangrove during neap tides. Finally, the results obtained from this study will make it possible to investigate in future research the sediment transport patterns, as well as the movements of other associated materials such as marine litter (very dense in coastal lagoons and estuaries with mangroves) and plastics debris, all of which present major challenges in the current environmental management of coastal ecosystems.

AKNOLEDGEMENTS

This work stems from the scientific collaboration between the Cheikh Anta Diop University (Dakar, Senegal) and La Rochelle University (France). Many thanks to Centre de Suivi Ecologique de Dakar and the Fond Français pour l'Environnement Mondiale (FFEM) as part of the West Africa Coastal Area (WACA) Program for finding this research. We would like to thank Alassane Touré Lemagnifique for his field assistance during all campaigns. Our thanks go to Jamal UDDIN KHAN, to Laura LAVAUD for their contributions during the model implementation at the LIENSs Laboratory (La Rochelle University) and to Denis DAUSSE for having prepared the pressure sensors that we deployed during our different field campaigns. Finally, we sincerely thank the two anonymous reviewers for their constructive comments, which improved the manuscript substantially.

REFERENCES

Albaret JJ, Diouf PS (1994) Diversité des poissons des lagunes et des estuaires ouest-africains. In : Teugels G.G. (ed.), Guégan Jean-François (ed.), Albaret Jean-Jacques (ed.). Biological diversity in African fresh- and brackish water fishes : geographical overviews : PARADI symposium = Diversité biologique des poissons des eaux douces et saumâtres d'Afrique : synthèses géographiques : symposium PARADI. Annales du Musée Royal d'Afrique Centrale. Sciences Zoologiques, 275, p. 165-177. Symposium PARADI, Saly (SEN), 1993/11/15-20.

Aubrey G (1986) Hydrodynamic Controls on Sediment Transport in Well-Mixed Bays and Estuaries. In Physics of Shallow Estuaries and Bays, J. van de Kreeke (Ed.). https://doi.org/10.1029/LN016p0245

Aucan J, Ridd P (2000) Tidal asymmetry in creeks surrounded by saltflats and mangroves with small swamp slopes. Wetlands Ecology and Management. 8. 223-232. 10.1023/A:1008459814925.

Baptist MJ, Babovic V, Uthurburu RJ, Keijzer M, Uittenbogaard RE, Mynett A, Verwey A (2007) On inducing equations for vegetation resistance. Journal of Hydraulic Research, 45(4), 435–450. https://doi.org/10.1080/00221686.2007.9521778

Barnes RSK (1980) Coastal Lagoons. Cambridge University Press. Cambridge, UK. 106 PP.

Bertin X, Fortunato AB, Dodet G (2015) Processes controlling the seasonal cycle of wave dominated inlets. Revista de Gestao Costeira Integrada-Journal of Integrated Coastal Zone Management 15, 9–19.

Bertin X, Fortunato AB, Oliveira A (2009) A modeling-based analysis of processes driving wave-dominated inlets. Continental Shelf Research, 29(5-6):819-834. DOI: 10.1016/j.csr.2008.12.019

Beudin A, Ganju NK, Defne Z, Aretxabaleta AL (2017b) Physical response of a back-barrier estuary to a post-tropical cyclone. J Geophys Res Oceans 122:5888–5904. https://doi.org/10.1002/2016JC012344

Beudin A, Kalra TS, Ganju NK, Warner JC (2017a) Development of a coupled wave-flow-vegetation interaction model. Comput Geosci. 100:76–86. https://doi.org/10.1016/j.cageo.2016.12.010

Biggs H, Nikora V, Papadopoulos K, Vettori D, Gibbins C, Kucher M (2016) Flow-vegetation interactions: A field study of ranunculus penicillatus at the large patch scale. Proceedings of the 11th international symposium on ecohydraulics, Melbourne, Australia. February, 7-12 P.

Brookes A, Shields FD (1996) River channel restoration: guiding principles for sustainable projects. Wiley, Chichester

Brown J, Davies A (2010) Flood/ebb tidal asymmetry in a shallow sandy estuary and the impact on net sand transport. Geomorphology 114 (3), 431–439.

Carrère L, Lyard F, Cancet M, Guillot A, Roblou L (2012) FES2012: A new global tidal model taking advantage of nearly 20 years of altimetry, *Proceedings of meeting "20 Years of Altimetry"*, Venice 2012.

Codiga D (2011) Unified tidal analysis and prediction using the UTide Matlab functions. 10.13140/RG.2.1.3761.2008.

Cromwell JE (1971) Barrier coast distribution: a world-wide survey. p. 50. Abstract. In: Second National Coastal Shallow Water Research Conference. Baton Rouge, LA.

Dahdouh-Guebas F, Jayatissa LP, Di Nitto D, Bosire JO, Lo Seen D, Koedam N (2005) How effective were mangroves as a defence against the recent tsunami? Curr Biol. 2005 Jun 21;15(12): R443-7. doi: 10.1016/j.cub.2005.06.008. Erratum in: Curr Biol. 2005 Jul 26;15(14):1337-8. PMID: 15964259.

Dahdouh-Guebas F, Koedam N (2008) Long-term retrospection on mangrove development using transdisciplinary approaches: a review. Aquatic Botany 89: 80–92

Day JW, Conner W, Ley-Lou F, Day R, Machado A (1987) The productivity and composition of mangrove forests, Laguna de Terminos, Mexico. Aquatic Botany 27: 267-284.

Dias JM, Valentim JM, Sousa MC (2013) A numerical study of local variations in tidal regime of Tagus estuary, Portugal. PLoS ONE 8(12): e80450. https://doi.org/10.1371/journal.pone.0080450

Dodet G, Bertin X, Bruneau B, Fortunato AB, Nahon A, Roland A (2013) Wave-current interactions in a wave-dominated tidal inlet. Journal of Geophysical Research: Oceans, 118(3):1587–1605. DOI: 10.1002/jgrc.20146

El Mahrad B, Newton A, Murray N (2022) Coastal Lagoons: Important Ecosystems. Front. Young Minds 10:637578. doi: 10.3389/frym.2022.637578

FAO (2007) The world's mangroves 1980–2005. Étude FAO: Forêts N° 153. Rome, FAO.

Fortunato AB, Oliveira A (2005) Influence of Intertidal Flats on Tidal Asymmetry. Journal of Coastal Research 215 (1), 1062–1067.

Friedrichs CT, Aubrey DG (1988) Non-linear tidal distortion in shallow well-mixed estuaries: a synthesis, Estuarine, Coastal and Shelf Science, Vol. 27, P.521-545.

Friedrichs CT, Lynch DR, Aubrey DG (1992) Velocity Asymmetries in Frictionally-Dominated Tidal Embayments. In Dynamics and Exchanges in Estuaries and the Coastal Zone, D. Prandle (Ed.). https://doi.org/10.1029/CE040p0277

Furukawa K, Wolanski E, Mueller H (1997) Currents and sediment transport in mangrove forests. Estuarine, Coastal and Shelf Science 1997, 44: 301–310.

GEBCO (2019) https://download.gebco.net/. Accessed 1 October 2020

Giri C, Ochieng E, Tieszen LL, Zhu Z, Singh A, Loveland T, Masek J, Duke N (2011) Status and distribution of mangrove forests of the world using earth observation satellite data. Glob. Ecol. Biogeogr. 2011, 20, 154–159.

Guerreiro M, Fortunato AB, Freire P, Rilo A, Taborda R, Freitas MC, Andrade C, Silva T, Rodrigues M, Bertin X, Azevedo A (2015) "Evolution of the hydrodynamics of the Tagus estuary (Portugal) in the 21st century", Revista de GestÃ£o Costeira Integrada, 15: 65 - 80. doi: 10.5894/rgci515

Horstman EM, Bryan KR, Mullarney JC (2021) Drag variations, tidal asymmetry and tidal range changes in a mangrove creek system. Earth Surf. Process. Landforms. 2021; 46: 1828– 1846. https://doi.org/10.1002/esp.5124

Horstman EM, Dohmen-Janssen CM, Bouma TJ, Hulscher SJ (2015) Tidal-scale flow routing and sedimentation in mangrove forests: combining field data and numerical modelling. Geomorphology, 228, 244–262. https://doi.org/10.1016/j.geomorph.2014.08.011

Horstman EM, Dohmen-Janssen CM, Hulscher SJ (2013) Modeling tidal dynamics in a mangrove creek catchment in Delft3D. In P. Bonneton, & T. Garlan (Eds.), Coastal Dynamics 2013: 24-28 June 2013, Arcachon, France (pp. 833-844). Bordeaux University - SHOM.

Horstman EM, Dohmen-Janssen CM, Narra PM, vandenBerg NJ, Siemerink M, Hulscher SJ (2014) Wave attenuation in mangroves: a quantitative approach to field observations. Coast Eng 94:47–62

Ji X, Huang L, Zhang W, Yao P (2022) On the Mechanism behind the Variation of the Tidal Current Asymmetry in Response to Reclamations in Lingding Bay, China. Journal of Marine Science and Engineering, 10(7), 951.

Kennish MJ, Paerl HW (2010) Coastal lagoons: critical habitats of environmental change. In Kennish, M. J., and Paerl, H. W. (eds.), Coastal Lagoons: Critical Habitats of Environmental Change. Boca Raton: CRC Press, pp. 1–15

Khan MJU, Ansary MN, Durand F, Testut L, Ishaque M, Calmant S, Krien Y, Islam AKMS, Papa F (2019) High-Resolution Intertidal Topography from Sentinel-2 Multi-Spectral Imagery: Synergy between Remote Sensing and Numerical Modeling. Remote Sensing. 11(24):2888. https://doi.org/10.3390/rs11242888

Kitheka JU (1997) Coastal tidally-driven circulation and the role of water exchange in the linkage between tropical coastal ecosystems. Estuarine, Coastal and Shelf Science 45, 177–187.

Kjerfve B (1994) Coastal lagoon processes. Coastal Lagoon Processes. 60. 1-8.

Kurniawan A, Hasan GM, Ooi SK, Lee WK, Leng L, Bayen S (2014) Understanding Hydrodynamic Flow Characteristics in a Model Mangrove Ecosystem in Singapore. Procedia APCBEE. 10. 286-291. 10.1016/j.apcbee.2014.10.054.

Lapetina A, Sheng YP (2014) Three-dimensional modeling of storm surge and inundation including the effects of coastal vegetation. Estuar Coasts 37:1028–1040

Lavaud L, Bertin X, Martins K, Arnaud G, Bouin MN (2020) The contribution of short-wave breaking to storm surges: The case Klaus in the Southern Bay of Biscay. Ocean Modelling. 156. 10.1016/j.ocemod.2020.101710.

Le Floch JF (1961) Propagation de la marée dynamique dans l'estuaire de la Seine et la Seine Maritime. Thèse, Paris, 507 p.

Lessa G, Masselink G (1995) Morphodynamic evolution of a macrotidal barrier estuary, Marine Geology, Volume 129, Issues 1–2, 1995, Pages 25-46, ISSN 0025-3227, https://doi.org/10.1016/0025-3227(95)00103-4.

Mazda Y, Kanazawa N, Wolanski E (1995) Tidal asymmetry in mangrove creeks. Hydrobiologia 295, 51–58.

Mazda Y, Kobashi D, Okada S (2005) Tidal-scale hydrodynamics within mangrove swamps. Wetlands Ecology and Management 2005, 13(6): 647-655.

Mazda Y, Magi M, Kogo M, Hong PN (1997) Mangroves as a coastal protection from waves in the Tong king delta, Vietnam. Mangroves Salt Marshes 1, 127–135. https:// doi.org/10.1023/A:1009928003700.

McIvor A, Spencer T, Möller I, Spalding M (2012) Storm surge reduction by mangroves. In Natural Coastal Protection Series: Report 2; The Nature Conservancy and Wetlands International: Cambridge, UK, 2012.

Miththapala S (2013) Lagoons and Estuaries. Coastal Ecosystems Series (Vol 4). vi + 73 pp. IUCN Sri Lanka Country Office, Colombo. ISBN: 978-955-0205-21-9

Moki H, Taguchi K, Nakagawa Y, Montani S, Kuwae T (2020) Spatial and seasonal impacts of submerged aquatic vegetation (SAV) drag force on hydrodynamics in shallow waters. *Journal of Marine Systems*, *209*, [103373]. https://doi.org/10.1016/j.jmarsys.2020.103373

Montgomery JM, Bryan KR, Horstman EM, Mullarney JC (2018) Attenuation of tides and surges by mangroves: contrasting case studies from New Zealand. Water, 10(9), 1119. https://doi.org/10.3390/w10091119

Montgomery JM, Bryan KR, Mullarney JC, Horstman EM (2019) Attenuation of storm surges by coastal mangroves. Geophysical Research Letters, 46(5), 2680–2689. https://doi.org/10.1029/2018gl081636

Nepf HM (1999) Drag, turbulence, and diffusion in flow through emergent vegetation. Water Resour Res 35:479–489

Nepf HM, Vivoni ER (2000) Flow structure in depth-limited, vegetated flow. J Geophys Res 105:28547. https://doi.org/10.1029/2000JC900145

Nguyen XT, Tanaka H, Umeda M, Sasaki M (2007) Winter Wave Setup at River Mouths Facing the Sea of Japan. PROCEEDINGS OF COASTAL ENGINEERING, JSCE. 55. 366-370. 10.2208/proce1989.55.366.

Norris BK, Mullarney JC, Bryan KR, Henderson SM (2017) The effect of pneumatophore density on turbulence: a field study in a Sonneratia-dominated mangrove forest. Vietnam. Cont. Shelf Res. 147, 114–127. https://doi.org/10.1016/ j.csr.2017.06.002.

Núñez P, Castanedo S, Medina R (2020) A global classification of astronomical tide asymmetry and periodicity using statistical and cluster analysis. Journal of Geophysical Research: Oceans, 125(8), e2020JC016143.

Núñez P, Castanedo S, Medina R (2021) Role of ocean tidal asymmetry and estuarine geometry in the fate of plastic debris from ocean sources within tidal estuaries. Estuarine, Coastal and Shelf Science, 259, 107470.

Olabarrieta M, Warner JC, Kumar N (2011) Wave-current interaction in Willapa Bay. Journal of Geophysical Research: Oceans 116. doi:10.1029/2011JC007387.

Oliveira A, Fortunato AB, Rego JRL (2006) Effect of morphological changes on the hydrodynamics and flushing properties of the Óbidos lagoon (Portugal). Continental Shelf Research, 26(8), 917–942. https://doi.org/10.1016/J.CSR.2006.02.011

Oliveira A, Fortunato AB, Rodrigues M, Azevedo A, Rogeiro J, Bernardo S, Lavaud L, Bertin X, Nahon A, DeJesus G, Rocha M, Lopes P (2021) Forecasting contrasting coastal and estuarine hydrodynamics with OPENCoastS, Environmental Modelling & Software, 143, 105132. https://doi.org/10.1016/j.envsoft.2021.105132

Pein JU, Stanev EV, Zhang Y (2014) The tidal asymmetries and residual flows in Ems Estuary, Ocean Dynamics, 64, 1719-41.

Picado A, Dias JM, Fortunato AB (2010) Tidal changes in estuarine systems induced by local geomorphologic modifications, Continental Shelf Res., 30/17: 1854-1864.

Saad S, Husain ML, Asano T (1999) Sediment accretion and variability of sedimentological characteristics of a tropical estuarine mangrove: Kemaman, Terengganu, Malaysia. Tropics 8, 257e266. *Mangroves and Salt Marshes, volume,3. Pages 51-58.*

Saha S, Moorthi S, Pan HL, Wu X, Wang J, Nadiga S, Tripp P, Kistler R, Woollen J, Behringer D et al (2010) The NCEP climate forecast system reanalysis. Bulletin of the American Meteorological Society 91, 1015–1058. doi:10.1175/2010BAMS3001.1.

Sakho I (2011) Évolution et fonctionnement hydro-sédimentaire de la lagune de la Somone, Petite Côte, Sénégal. Sciences de l'environnement. Thèse de doctorat. Université de Rouen ; Université Cheikh Anta Diop de Dakar, Sénégal.

Sakho I, Mesnage V, Deloffre J, Lafite R, Niang I, Faye G (2011) The influence of natural and anthropogenic factors on mangrove dynamics over 60 years: The Somone Estuary, Senegal. Estuarine, Coastal and Shelf Science, 94, 93-101.

Sakho I, Sadio M, Camara I, Noblet M, Seck A, Saengsupavanich C, Ndour A, Diouf MB (2022) Sea level rise and future shoreline changes along the sandy coast of Saloum Delta, Senegal. *Arab J Geosci* 15, 1547. https://doi.org/10.1007/s12517-022-10741-y

Sathyanathan R, Deeptha T (2013) Numerical Simulation of Tidal Circulation in the Pichavaram Mangrove Estuary. International Journal of Research in Engineering and Technology, eISSN: 2319-1163 | pISSN: 2321-7308

Shan Y, Liu C, Nepf HM (2019) Comparison of drag and velocity in model mangrove forests with random and in-line tree distributions, Journal of Hydrology, Volume 568, Pages 735-746, ISSN 0022-1694, https://doi.org/10.1016/j.jhydrol.2018.10.077.

Song D, Wang X, Kiss A, Bao, X (2011) The contribution to tidal asymmetry by different combinations of tidal constituents. Journal of Geophysical Research, 116, C12007. https://doi.org/10.1029/2011JC007270

Sousa A, Garcia-Murillo P, Morales J, García-Barrón L (2009) Anthropogenic and natural effects on the coastal lagoons in the southwest of Spain (Doñana National Park). ICES Journal of Marine Science. 66. 1508-1514. 10.1093/icesjms/fsp106.

Spalding MD, Blasco F, Field CD (1997) World Mangrove Atlas. International Society for Mangrove Ecosystems, Okinawa (Japan), 178 pp.

Stutz ML, Pilkey OH (2001) A review of global barrier island distribution. Journal of Coastal Research. 34. 15-22.

Stutz ML, Pilkey OH (2011) Open-ocean barrier islands: global influence of climatic, oceanographic, and depositional settings. Journal of Coastal Research, 27(2), 207–222. West Palm Beach (Florida), ISSN 0749-0208. https://doi.org/10.2112/09-1190.1

Temmerman S, Bouma TJ, Govers G, Wang ZB, De Vries MB, Herman PMJ (2005) Impact of vegetation on flow routing and sedimentation patterns: three-dimensional modeling for a tidal marsh. J Geophys Res 110 : F04019. https://doi.org/10.1029/2005JF000301

Wang ZB, Jeuken CJ, De Vriend HJ (1999) Tidal asymmetry and residual sediment transport in estuaries: a literature study and application to the Western Scheldt. Delft Hydraulics: Delft. 66 pp.

Webster IT, Harris GP (2004) Anthropogenic impacts on the ecosystems of coastal lagoons: Modelling fundamental biogeochemical processes and management implications. Marine and Freshwater Research, 55, 67-78.

Wolanski E (1992) Hydrodynamics of mangrove swamps and their coastal waters. *Hydrobiologia* 247, 141–161. https://doi.org/10.1007/BF00008214

Wolanski E, Jones M, Bunt JS (1980) Hydrodynamics of a tidal creek–mangrove swamp system. Australian Journal of Marine and Freshwater Research 31, 431–450.

Wolanski E, Mazda Y, King B, Gay S (1990) Dynamics, flushing and trapping in Hinchinbrook Channel, a giant mangrove swamp, Australia. Estuarine, Coastal and Shelf Science 31, 555–579

Wu Y, Falconer RA, Struve J (2001) Mathematical modelling of tidal currents in mangrove forests. Environmental Modelling and Software. 16.19-29.

Yoshikai M, Nakamura T, Bautista DM, Herrera EC, Baloloy A, Suwa R et al (2022) Field measurement and prediction of drag in a planted Rhizophora mangrove forest. Journal of Geophysical Research: Oceans, 127, e2021JC018320. https://doi.org/10.1029/2021JC018320

Zapata C, Puente A, García A, García-Alba J, Espinoza J (2019) The Use of Hydrodynamic Models in the Determination of the Chart Datum Shape in a Tropical Estuary. *Water*. 11(5):902. https://doi.org/10.3390/w11050902

Zhang Y, Ye F, Stanev EV, Grashorn S (2016) Seamless cross-scale modeling with SCHISM, Ocean Modelling, 102, 64-81.

Zhang YJ, Gerdts N, Ateljevich E, Nam K (2020) Simulating vegetation effects on flows in 3D using an unstructured grid model: model development and validation. *Ocean Dynamics* 70, 213–230. https://doi.org/10.1007/s10236-019-01333-8